

# Improving physics-informed DeepONets with hard constraints

Rüdiger Brecht<sup>†</sup>, Dmytro R. Popovych<sup>‡,§</sup>, Alex Bihlo<sup>‡</sup> and Roman O. Popovych<sup>‡,§</sup>

<sup>†</sup>*Department of Mathematics, University of Hamburg, Hamburg, Germany*

<sup>‡</sup> *Department of Mathematics and Statistics, Memorial University of Newfoundland, St. John's (NL) A1C 5S7, Canada*

<sup>§</sup> *Mathematical Institute in Opava, Silesian University in Opava, Na Rybnicku 626/1, 746 01 Opava, Czech Republic*

<sup>§</sup> *Institute of Mathematics of NAS of Ukraine, 3 Tereshchenkivska Str., 01024 Kyiv, Ukraine*

E-mails: [ruediger.brecht@uni-hamburg.de](mailto:ruediger.brecht@uni-hamburg.de), [dpopovych@mun.ca](mailto:dpopovych@mun.ca),  
[abihlo@mun.ca](mailto:abihlo@mun.ca), [rop@imath.kiev.ua](mailto:rop@imath.kiev.ua)

Current physics-informed (standard or operator) neural networks still rely on accurately learning the initial conditions of the system they are solving. In contrast, standard numerical methods evolve such initial conditions without needing to learn these. In this study, we propose to improve current physics-informed deep learning strategies such that initial conditions do not need to be learned and are represented exactly in the predicted solution. Moreover, this method guarantees that when a DeepONet is applied multiple times to time step a solution, the resulting function is continuous.

## 1 Introduction

Recent years have seen tremendous interest in solving differential equations with neural networks. Originally introduced in [7] and popularized through [12], in which it is referred to as the method *physics-informed neural networks*, it has become popular throughout the mathematical sciences, with applications to astronomy [11], biomedical engineering [8], geophysics [13] and meteorology [3], just to name a few.

While the underlying method is conceptually straightforward to implement, several failure modes of the original method have been identified in the past [2, 6, 15, 16, 18], along with some mitigation strategies.

Setting these training difficulties aside, another fundamental shortcoming of physics-informed neural networks is that they require extensive training, to the point where they are seldom computationally competitive compared to standard numerical methods, see [4] for an example related to weather prediction. The main issue is that each changing of initial and/or boundary conditions for a system of differential equations requires retraining of the neural network solution approximator, which is a costly endeavour, especially when accurate solutions are required.

One strategy to overcome this issue is to not learn the solution of a differential equation itself, but rather the solution operator. This idea, relying on the universal approximation theorem for operators [5], was proposed in [10], where it is referred to as *physics-informed deep operator approach*, or *physics-informed DeepONet*. The main idea is that a physics-informed DeepONet, which in the following we will simply refer to as DeepONet, accepts both the initial/boundary

data and the independent variables of the differential equation to be solved, and learns to approximate the solution operator of that differential equation for any given initial/boundary conditions. Once trained, a DeepONet can thus simply be evaluated for varying initial/boundary conditions, with no other cost than inference of the neural network. A notable advantage of this approach is that it allows time-stepping for time-dependent differential equations [14], which overcomes the failure mode of physics-informed neural networks that tend to converge to a trivial solution when trained for long time intervals. Thus, rather than solving a differential equation over the entire time interval with a single neural network, one trains a DeepONet over a shorter time interval and then repeatedly evaluates the DeepONet, using as new initial condition the final solution from the previous iteration step. This makes numerical methods based on DeepONets similar to more traditional numerical techniques such as Runge–Kutta methods or linear multistep methods.

While DeepONets have the potential to make neural network based differential equations solver computationally more efficient, they still suffer from some of the same training difficulties as standard physics-informed neural networks. Among all training difficulties, one of the most challenging one to address is that the minimization problem to be solved for both physics-informed neural networks and DeepONets is typically formulated based on a non-convex, composite multi-task loss function. Here, the multiple tasks refer to simultaneously minimizing loss components associated with the differential equation and all initial and boundary conditions, respectively.

However, already the original work by [7] has shown that the minimization problem to be solved can be simplified by including these initial and/or boundary conditions as hard constraints to the neural network. Still, the prevalent way of solving both physics-informed neural networks and DeepONets relies on including these initial and/or boundary conditions in the loss function as a soft constraint. The aim of this paper is to present a comprehensive comparison between the two approaches, and to show that the hard-constraint approach is vastly superior to the soft-constraint approach for DeepONets.

The further organization of this paper is as follows. In Section 2 we review the use of neural networks for solving differential equations, using physics-informed neural networks and DeepONets. Here we focus on both the soft and hard constraint formulations. In Section 3 we show some comparison for soft- and hard-constrained DeepONets solving some important benchmark problems such as the damped pendulum, the Poisson equation and the Korteweg–de Vries equation. The final Section 4 contains a summary of our work together with some possible further research avenues.

## 2 Solving differential equations with neural networks

In this section, we review the ideas of physics-informed neural networks and deep operator networks. For this, we consider the general form of a boundary value problem for a system of differential equation defined over the domain  $\Omega$ ,

$$\Delta^l(\mathbf{x}, \mathbf{u}_{(n)}) = 0, \quad l = 1, \dots, L, \quad \mathbf{x} \in \Omega, \quad (1a)$$

$$\mathbf{B}^{l_b}(t, \mathbf{x}, \mathbf{u}_{(n_b)}) = 0, \quad l_b = 1, \dots, L_b, \quad \mathbf{x} \in \partial\Omega, \quad (1b)$$

Here  $\mathbf{x} = (x_1, \dots, x_d)$  is the tuple of independent variables,  $\Omega \subset \mathbb{R}^d$ ,  $\mathbf{u} = \mathbf{u}(\mathbf{x}) = (u^1, \dots, u^q)$  denotes the tuple of dependent variables, and  $\mathbf{u}_{(n)}$  denotes the tuple of derivatives of the de-

pendent variables  $\mathbf{u}$  with respect to the independent variables  $\mathbf{x}$  of order not greater than  $n$ .  $\mathbf{B} = (\mathbf{B}^1, \dots, \mathbf{B}^{L_b})$  denotes the boundary value operator,  $L_b \in \mathbb{N} := \{1, 2, \dots\}$ .

There are various more specific versions of the general form (1) for particular classes of boundary value problems. Thus, if an independent variable is singled out in the entire tuple of independent variables as the time, we can re-denote the number of independent variables as  $d + 1$ , start numbering them from zero and assume  $x_0$  as the time variable,  $x_0 := t$ . Then the general boundary value problem (1) is converted into an initial-boundary value problem over the spatio-temporal domain  $\Omega = [t_0, t_f] \times \Omega'$ , where  $[t_0, t_f]$  and  $\Omega' \subset \mathbb{R}^d$  are the interval and the domain run by the time variable  $t$  and the spatial variables  $\mathbf{x} = (x_1, \dots, x_d)$ , respectively, and the general boundary conditions (1b) split into initial conditions at  $t = t_0$  and (spatial) boundary conditions at the boundary  $\partial\Omega'$  of  $\Omega'$ ,

$$\begin{aligned} \Delta^l(t, \mathbf{x}, \mathbf{u}_{(n)}) &= 0, \quad l = 1, \dots, L, \quad t \in [t_0, t_f], \quad \mathbf{x} \in \Omega', \\ \mathbf{I}^{l_i}(\mathbf{x}, \mathbf{u}_{(n_i)}|_{t=t_0}) &= 0, \quad l_i = 1, \dots, L_i, \quad \mathbf{x} \in \Omega', \\ \mathbf{B}_s^{l_{sb}}(t, \mathbf{x}, \mathbf{u}_{(n_{sb})}) &= 0, \quad l_{sb} = 1, \dots, L_{sb}, \quad t \in [t_0, t_f], \quad \mathbf{x} \in \partial\Omega', \end{aligned} \quad (2)$$

Here,  $\mathbf{I} = (\mathbf{I}^1, \dots, \mathbf{I}^{L_i})$  is the initial value operator and  $\mathbf{B}_s = (\mathbf{B}_s^1, \dots, \mathbf{B}_s^{L_{sb}})$  denotes the (spatial) boundary value operator.

In particular, for a system of evolution equations, one has  $L = q$ ,  $\Delta^l = u_t^l - \tilde{\Delta}^l(t, \mathbf{x}, \mathbf{u}_{(x,n)})$  and  $\mathbf{I} = \mathbf{u}|_{t=t_0} - \mathbf{f}(\mathbf{x})$ , where  $\mathbf{u}_{(x,n)}$  denotes the tuple of derivatives of the dependent variables with respect to the spatial independent variables of order not greater than  $n$ ,  $u_t^l := \partial u^l / \partial t$ , and  $\mathbf{f}(\mathbf{x}) = (f^1(\mathbf{x}), \dots, f^q(\mathbf{x}))$  is a fixed vector function of  $\mathbf{x}$  with the domain  $\Omega'$ . For a system of differential equations that involves at most double differentiation with respect to  $t$  and can be solved with respect to  $\partial^2 u^l / \partial t^2$ , one also has  $L = q$ , and the initial value operator is  $\mathbf{I} = (\mathbf{u}|_{t=t_0} - \mathbf{f}(\mathbf{x}), \mathbf{u}_t|_{t=t_0} - \tilde{\mathbf{f}}(\mathbf{x}))$ , where  $\tilde{\mathbf{f}}(\mathbf{x}) = (\tilde{f}^1(\mathbf{x}), \dots, \tilde{f}^q(\mathbf{x}))$  is one more fixed vector function of  $\mathbf{x}$  with the domain  $\Omega'$ . If  $n = 2$ , a possible choice for boundary conditions is given by Dirichlet boundary conditions, where  $\mathbf{B}_s = \mathbf{u} - \mathbf{g}(t, \mathbf{x})$  for a fixed vector function  $\mathbf{g}(t, \mathbf{x}) = (g^1(t, \mathbf{x}), \dots, g^q(t, \mathbf{x}))$  with the domain  $[t_0, t_f] \times \partial\Omega'$ . Of course, there are many other kinds of boundary conditions that are relevant for applications (Neumann boundary conditions, mixed boundary conditions, periodic boundary conditions, etc.). In the case of systems of ordinary differential equations, where  $d = 0$ , one can consider purely initial value problems without boundary conditions or, conversely, boundary value problems of the general form, including multipoint boundary value problems.

## 2.1 Physics-informed neural networks

Let  $\mathbf{u}^\theta(t, \mathbf{x})$  be the output of a deep neural network with inputs  $\mathbf{x}$  and trainable parameters (weights)  $\theta$  that approximates the solution  $\mathbf{u}$  of the boundary value problem (1). The network can be trained over the neural network parameters  $\theta$  using the composite loss function

$$\mathcal{L}(\theta) = \lambda_\Delta \mathcal{L}_\Delta(\theta) + \lambda_b \mathcal{L}_b(\theta) \quad (3)$$

with

$$\mathcal{L}_\Delta(\theta) = \frac{1}{N_\Delta} \sum_{i=1}^{N_\Delta} \sum_{l=1}^L |\Delta^l(\mathbf{x}_\Delta^i, \mathbf{u}_\theta^{(n)}(\mathbf{x}_\Delta^i))|^2,$$

$$\mathcal{L}_b(\theta) = \frac{1}{N_b} \sum_{i=1}^{N_b} \sum_{l_b=1}^{L_b} |\mathbf{B}^{l_b}(\mathbf{x}_b^i, \mathbf{u}_\theta^{(n_b)}(\mathbf{x}_b^i))|^2$$

are the equation loss and the boundary value loss, respectively. The parameters  $\lambda_\Delta, \lambda_b \in \mathbb{R}_{>0}$  are the loss weights, which also can be assigned as trainable. The above losses are standard mean-squared errors computed at the sets of collocation points  $\{\mathbf{x}_\Delta^i\}_{i=1}^{N_\Delta} \subset \Omega$  and  $\{\mathbf{x}_b^i\}_{i=1}^{N_b} \subset \partial\Omega$  for the system  $\Delta$  and for the boundary conditions, respectively. The approximation of the solution  $\mathbf{u}$  of the boundary value problem (1) by the output  $\mathbf{u}^\theta(t, \mathbf{x})$  of the deep neural network is ensured by enforcing the simultaneous minimization of both losses. In practice, when computing within the framework of mini-batch gradient descent, the collocation points are partitioned into subsets called batches. Every iteration over the entire set of collocation points, called an epoch, consists of multiple gradient descent steps, each carried out using the loss computed for the respective batch.

An important advantage of neural networks over standard numerical approximations lies in computing derivatives using automatic differentiation [1]. This gives exact derivatives avoiding discretization error, so that the only error stemming from finite-precision arithmetic.

When considering a particular boundary value problem, the structure of loss function (3) for the general case, including the number of its components, should often be modified for taking into account specific features of the problem under consideration. Thus, for the initial-boundary value problem (2), it is natural to split the common boundary value loss into two parts, the initial value loss  $\mathcal{L}_i(\theta)$  and the spacial boundary value loss  $\mathcal{L}_{sb}(\theta)$ . In other words, the loss function in this case can be represented as

$$\mathcal{L}(\theta) = \lambda_\Delta \mathcal{L}_\Delta(\theta) + \lambda_i \mathcal{L}_i(\theta) + \lambda_{sb} \mathcal{L}_{sb}(\theta), \quad (4)$$

with

$$\begin{aligned} \mathcal{L}_\Delta(\theta) &= \frac{1}{N_\Delta} \sum_{i=1}^{N_\Delta} \sum_{l=1}^L |\Delta^l(t_\Delta^i, \mathbf{x}_\Delta^i, \mathbf{u}_{(n)}^\theta(t_\Delta^i, \mathbf{x}_\Delta^i))|^2, \quad (t_\Delta^i, \mathbf{x}_\Delta^i) \in [t_0, t_f] \times \Omega', \quad i = 1, \dots, N_\Delta, \\ \mathcal{L}_i(\theta) &= \frac{1}{N_i} \sum_{i=1}^{N_i} \sum_{l_i=1}^{L_i} |l_i(\mathbf{x}_i^i, \mathbf{u}_{(n_i)}^\theta(t_0, \mathbf{x}_i^i))|^2, \quad \mathbf{x}_i^i \in \Omega', \quad i = 1, \dots, N_i, \\ \mathcal{L}_{sb}(\theta) &= \frac{1}{N_{sb}} \sum_{i=1}^{N_{sb}} \sum_{l_{sb}=1}^{L_{sb}} |\mathbf{B}_s^{l_{sb}}(t_{sb}^i, \mathbf{x}_{sb}^i, \mathbf{u}_{(n_{sb})}^\theta(t_{sb}^i, \mathbf{x}_{sb}^i))|^2, \\ &\quad (t_{sb}^i, \mathbf{x}_{sb}^i) \in [t_0, t_f] \times \partial\Omega', \quad i = 1, \dots, N_{sb}. \end{aligned}$$

Moreover, the loss function for an initial value problem for a system of ordinary differential equations has no component  $\mathcal{L}_{sb}$ .

Although physics-informed neural networks give a promising way to approximate solutions of boundary value problem, they can fail, e.g., for initial-boundary value problems with long time intervals [14]. One way to overcome the problem for long-term integration is to learn mappings from initial data to the associated solutions of the corresponding initial-boundary value problems. This can be achieved within the DeepONet framework.

## 2.2 Deep operator neural networks with soft constraint

DeepONets are designed to approximate (non)linear operators between compact subsets of (finite- or infinite-dimensional) Banach spaces, which are usually functional spaces. The DeepONet architecture that is commonly considered in the literature includes two main components, the *branch net* and the *trunk net*. The branch and trunk nets are respectively responsible for

encoding the dependence of the output function on the input parameter functions (typically restricted to fixed finite subsets of their domains) and its arguments. Convolving the outcomes of the branch and trunk networks with a trainable constant rank-two tensor gives the output of the DeepONet.

We specify abstract DeepONets to the particular case of mappings between boundary data and solutions of the corresponding boundary value problems for a fixed system of differential equations. More specifically, we consider a parameterized family of boundary value problems of the general form (1),

$$\Delta^l(\mathbf{x}, \mathbf{u}_{(n)}) = 0, \quad l = 1, \dots, L, \quad \mathbf{x} \in \Omega, \quad (5a)$$

$$\mathbf{B}^{l_b}(t, \mathbf{x}, \mathbf{u}_{(n_b)}, \boldsymbol{\varphi}) = 0, \quad l_b = 1, \dots, L_b, \quad \mathbf{x} \in \partial\Omega, \quad (5b)$$

where the boundary conditions are parameterized by a tuple of parameter functions  $\boldsymbol{\varphi} = \boldsymbol{\varphi}(\mathbf{x}) = (\varphi^1, \dots, \varphi^{L_p})$  running through a compact (with respect to a metric) set  $\mathcal{M}$  of sufficiently smooth function  $L_p$ -tuples with domain  $\partial\Omega$ .<sup>1</sup>

To encode the varying boundary data, we evaluate the function tuple  $\boldsymbol{\varphi}$  at the set of  $N_s$  sensor points  $\mathcal{S} := \{\mathbf{x}_s^i\}_{i=1}^{N_s} \subset \partial\Omega$ ,  $\boldsymbol{\Phi} := (\boldsymbol{\varphi}(\mathbf{x}_s^1), \dots, \boldsymbol{\varphi}(\mathbf{x}_s^{N_s}))$ .<sup>2</sup> Then a standard DeepONet  $\mathcal{G}^\theta$  takes the form [10]

$$\mathcal{G}^\theta(\boldsymbol{\Phi})(\mathbf{x}) = \sum_{i,j} \check{\boldsymbol{\theta}}_{ij} \mathcal{B}_i^\theta(\boldsymbol{\Phi}) \mathcal{T}_j^\theta(\mathbf{x}), \quad (6)$$

where  $\mathcal{B}_i^\theta$  and  $\mathcal{T}_j^\theta$  are the embedded outputs of the branch and trunk nets, and  $\boldsymbol{\theta} = (\check{\boldsymbol{\theta}}, \hat{\boldsymbol{\theta}}, \check{\boldsymbol{\theta}})$  is the complete tuples of network weights.

To define the loss function for training the DeepONet  $\mathcal{G}^\theta$ , in addition to sampling collocation points in  $\Omega$  and  $\partial\Omega$ , one needs to sample function tuples  $\boldsymbol{\varphi}^1, \dots, \boldsymbol{\varphi}^{N_f}$  in the set  $\mathcal{M}$ . Denote  $\boldsymbol{\Phi}^{l_f} := (\boldsymbol{\varphi}^{l_f}(\mathbf{x}_s^1), \dots, \boldsymbol{\varphi}^{l_f}(\mathbf{x}_s^{N_s}))$ ,  $l_f = 1, \dots, N_f$ . The parts of the physics-informed loss (3) are modified as follows:

$$\begin{aligned} \mathcal{L}_\Delta(\boldsymbol{\theta}) &= \frac{1}{N_f} \frac{1}{N_\Delta} \sum_{l_f=1}^{N_f} \sum_{i=1}^{N_\Delta} \sum_{l=1}^L |\Delta^l(\mathbf{x}_\Delta^i, \mathcal{G}^\theta(\boldsymbol{\Phi}^{l_f})_{(n)}(\mathbf{x}_\Delta^i))|^2, \\ \mathcal{L}_b(\boldsymbol{\theta}) &= \frac{1}{N_f} \frac{1}{N_b} \sum_{l_f=1}^{N_f} \sum_{i=1}^{N_b} \sum_{l_b=1}^{L_b} |\mathbf{B}^{l_b}(\mathbf{x}_b^i, \mathcal{G}^\theta(\boldsymbol{\Phi}^{l_f})_{(n_b)}(\mathbf{x}_b^i))|^2. \end{aligned}$$

Modifications of the loss function that are required for more specific value problems are obvious.

The above architecture overcomes some of the problems of the physics-informed neural network. However, in this setup DeepONets still need to learn initial and/or boundary conditions of the problems under consideration.

<sup>1</sup>In general, the boundary value operator  $\mathbf{B}$  may involve derivatives of  $\boldsymbol{\varphi}$  with respect to  $x$  as well. Moreover, the system (5a) may also be parameterized in a similar way by functions with domain  $\Omega$ .

<sup>2</sup>This is not the only possible way to encode the boundary data. Indeed, either the set  $\mathcal{M}$  is parameterized by a finite number of parameters, or we can approximate elements of  $\mathcal{M}$  by elements of a family  $\mathcal{M}'$  of functions with a finite number of parameters. These parameters can be used directly to encode the boundary conditions for the network instead of values of functions from  $\mathcal{M}$  in sensor points. This is always the case for initial or boundary value conditions for ordinary differential equations due to their parameterization at most by constants.

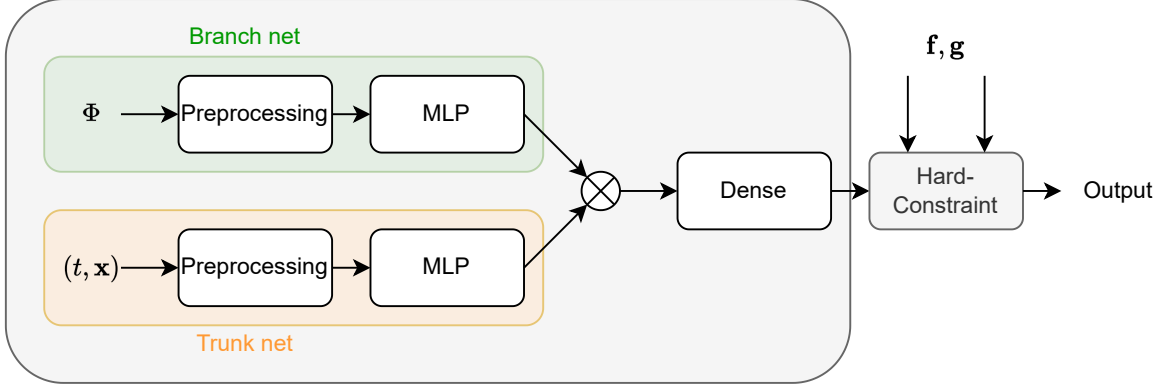


Figure 1. Overview of the used neural network architecture. Here, multilayer perceptron is abbreviated by MLP.

### 2.3 DeepONets with hard constraints

Here, we discuss DeepONets with hard constraints by way of the example of a family of initial-boundary value problems of the form (2) for systems of evolution equations with Dirichlet boundary conditions.<sup>3</sup> Thus,

$$L = q, \quad \Delta^l = u_t^l - \tilde{\Delta}^l(t, \mathbf{x}, \mathbf{u}_{(\mathbf{x}, n)}), \quad \mathbf{I} = \mathbf{u}|_{t=t_0} - \mathbf{f}(\mathbf{x}), \quad \mathbf{B}_s = \mathbf{u} - \mathbf{g}(t, \mathbf{x}), \quad (7)$$

and hence the parameter-function tuple is  $\varphi = (\mathbf{f}, \mathbf{g})$  with  $\mathbf{f}: (\Omega' \cup \partial\Omega') \rightarrow \mathbb{R}^q$  and  $\mathbf{g}: [t_0, t_f] \times \partial\Omega' \rightarrow \mathbb{R}^q$ . The consistency of initial and boundary conditions means that  $\mathbf{f}(\mathbf{x}) = \mathbf{g}(t_0, \mathbf{x})$ ,  $\mathbf{x} \in \partial\Omega'$ . The set of sensor points  $\mathcal{S}$  naturally splits into two subsets, the subset  $\mathcal{S}_i := \{\mathbf{x}_{s,i}^i\}_{i=1}^{N_{s,i}} \subset \Omega'$  of sensor points for the initial conditions and the subset  $\mathcal{S}_{sb} := \{\mathbf{x}_{s,sb}^i\}_{i=1}^{N_{s,sb}} \subset [t_0, t_f] \times \partial\Omega'$  of sensor points for the spatial boundary conditions,  $N_s = N_{s,i} + N_{s,sb}$ . Then  $\Phi = (\Phi_i, \Phi_{sb})$ , where  $\Phi_i := \mathbf{f}(\mathcal{S}_i)$  and  $\Phi_{sb} := \mathbf{g}(\mathcal{S}_{sb})$ .

We propose to implement hard constraints either directly in the architecture of the DeepONet, see Fig. 1, or in the loss function, such that initial and boundary conditions are exactly met.

Consider a DeepONet  $\mathcal{G}^\theta(\mathbf{f}, \mathbf{g}; \Phi)(t, \mathbf{x})$  with a hard-constraint layer that enforces the initial and spatial boundary conditions. Thus, the final output is, e.g.,

$$\mathcal{G}^\theta(\mathbf{f}, \mathbf{g}; \Phi)(t, \mathbf{x}) = F_i(t, \mathbf{x})\mathbf{f}(\mathbf{x}) + F_{sb}(t, \mathbf{x}) + F_{nn}(t, \mathbf{x})\mathcal{G}_t^\theta(\mathbf{f}, \mathbf{g}; \Phi)(t, \mathbf{x}), \quad (8)$$

where  $(t, \mathbf{x}) \in [t_0, t_f] \times (\Omega' \cup \partial\Omega')$ ,  $\mathcal{G}_t^\theta$  is the trainable part of the network  $\mathcal{G}^\theta$ , and  $F_i$ ,  $F_{sb}$  and  $F_{nn}$  are fixed sufficiently smooth functions with domain  $[t_0, t_f] \times (\Omega' \cup \partial\Omega')$  that satisfy the conditions

$$F_i(t_0, \mathbf{x}) = 1, \quad F_{nn}(t_0, \mathbf{x}) = 0, \quad \frac{\partial F_{nn}}{\partial t}(t_0, \mathbf{x}) \neq 0, \quad \mathbf{x} \in \Omega', \quad (9)$$

$$F_{sb}(t, \mathbf{x}) = \mathbf{g}(t, \mathbf{x}) - F_i(t, \mathbf{x})\mathbf{f}(\mathbf{x}), \quad F_{nn}(t, \mathbf{x}) = 0, \quad (t, \mathbf{x}) \in [t_0, t_f] \times \partial\Omega', \quad (10)$$

$$F_{nn}(t, \mathbf{x}) \neq 0, \quad (t, \mathbf{x}) \in (t_0, t_f] \times \Omega'. \quad (11)$$

This way we guarantee

$$\begin{aligned} \mathcal{G}^\theta(\mathbf{f}, \mathbf{g}; \Phi)(t_0, \mathbf{x}) &= \mathbf{f}(\mathbf{x}), \quad \mathbf{x} \in \Omega', \\ \mathcal{G}^\theta(\mathbf{f}, \mathbf{g}; \Phi)(t, \mathbf{x}) &= \mathbf{g}(t, \mathbf{x}), \quad (t, \mathbf{x}) \in [t_0, t_f] \times \partial\Omega'. \end{aligned} \quad (12)$$

<sup>3</sup>See examples of possible hard-constraint ansatzes for other kinds of boundary value problems in [7]. There is a great variety of such ansatzes even for a specific boundary value problem, cf. Remark 1. We plan to discuss selecting them in a forthcoming paper.

Therefore, the network  $\mathcal{G}^\theta$  can be trained over the neural network parameters  $\theta$  using the one-component loss function including only the equation loss,  $\mathcal{L}(\theta) = \mathcal{L}_\Delta(\theta)$ . This constitutes the main advantage of hard-constrained DeepONets over soft-constrained ones.

**Remark 1.** Other forms of hard constraints that are more specific or more general than (8) can be considered. In particular, the function  $F_i$  can be assumed to depend only on  $t$  or even to be the constant function 1 or, on the other hand, to be a  $q \times q$  matrix function with  $F_i(t_0, \mathbf{x})$  equal to the  $q \times q$  unit matrix.

It often happens that the solution of the problem (2) is not well approximated by a PINN. In this case, one can try to partition the entire interval  $[t_0, t_f]$  into subintervals  $[t_{j-1}, t_j]$ ,  $j = 1, \dots, k$  with  $t_0 < t_1 < \dots < t_k = t_f$ ,  $k > 0$  and solve the sequence of initial-boundary value problems on these subintervals using the evaluation of the solution of the  $j$ th problem at  $t = t_j$  as the initial condition for the  $(j+1)$ th problem. This is the essence of the time-stepping procedure. Of course, the best choice here is given by the partition into intervals of the same length  $\Delta t$ . The time-stepping can be efficiently realized within the framework of DeepONets considering  $t_0$  as one more parameter of the network to be used, training the network for the network over the interval  $[t_0, t_0 + \Delta t]$  and substituting  $t_0 + (j-1)\Delta t$  instead of  $t_0$  in the  $j$ th step of the time-stepping procedure. If the system of differential equations in (2) is invariant with respect to translations in  $t$  and the parameter function  $\mathbf{g}$  in the spatial boundary conditions does not depend on  $t$ , then the time-stepping procedure is even simpler since it does not require modifying the network by extending the parameter set of the network with  $t_0$ .

The approximate solution of the problem (2) in the particular setting (7) using the time-stepping procedure for the modified hard-constrained DeepONet (8) with the additional parameter  $t_0$  takes the form

$$\Gamma(t, x) = \mathcal{G}^\theta(t_{j-1}, \mathbf{f}^{j-1}, \mathbf{g}; \Phi^j)(t, \mathbf{x}), \quad (t, \mathbf{x}) \in [t_{j-1}, t_j] \times (\Omega' \cup \partial\Omega'), \quad j = 1, \dots, k,$$

where  $\mathbf{f}^0 := \mathbf{f}$ ,  $\mathbf{f}^j := \mathcal{G}^\theta(t_{j-1}, \mathbf{f}^{j-1}, \mathbf{g}; \Phi^j)(t_j, \cdot)$ ,  $j = 1, \dots, k-1$ ,

$$\mathcal{S}_i^j := \{\mathbf{x}_{s,i}^{j,i}\}_{i=1}^{N_{s,i}^j} \subset \Omega', \quad \mathcal{S}_{sb}^j := \{\mathbf{x}_{s,sb}^{j,i}\}_{i=1}^{N_{s,sb}^j} \subset [t_{j-1}, t_j] \times \partial\Omega'$$

are the sets of sensor points for the initial and the spacial boundary conditions of the  $j$ th problem, respectively,  $\Phi^j = (\Phi_i^j, \Phi_{sb}^j)$  with  $\Phi_i^j := \mathbf{f}(\mathcal{S}_i^j)$  and  $\Phi_{sb}^j := \mathbf{g}(\mathcal{S}_{sb}^j)$ ,  $j = 1, \dots, k$ . For simplicity, one can choose  $\mathcal{S}_i^1 = \dots = \mathcal{S}_i^k := \mathcal{S}_i$ . In the case of partition into intervals of the same length  $\Delta t$ , one can obtain the sensor-point sets  $\mathcal{S}_{sb}^j$ ,  $j = 2, \dots, k$  by means of successively shifting the first sensor-point set  $\mathcal{S}_{sb}^1$  in  $\Delta t$  in the  $t$ -direction. In view of (12) and the construction of the function  $\Gamma$ , this function is at least a continuous function on  $[t_0, t_f] \times (\Omega' \cup \partial\Omega')$ . Moreover, a greater order of smoothness of the function  $\Gamma$  can be enforced by a proper choice of the functions  $F_i$ ,  $F_{sb}$ ,  $F_{nn}$  and the activation function.

**Example 1** (Dirichlet boundary condition in 1D). Consider a family of initial-boundary value problems with  $d = 1$ ,  $q = 1$ ,  $\Omega' = [0, 1]$  and Dirichlet boundary condition for a single evolution equation. Thus,  $\mathbf{l} = u(t_0, x) - f(x)$ ,  $\mathbf{B}_s = (u(t, 0) - g^0(t), u(t, 1) - g^1(t))$ , and the consistency of initial and boundary conditions implies that  $g^0(t_0) = f(0)$  and  $g^1(t_0) = f(1)$ . We can set  $F_i \equiv 1$ ,  $F_{sb}(t, x) = (g^0(t) - f(0))(1 - x) + (g^1(t) - f(1))x$  and  $F_{nn}(t, x) = tx(x - 1)$ .

We note that depending on the choice of  $(F_i, F_{sb}, F_{nn})$  the outcome of the training can be better or worse.

**Remark 2.** The case of systems of ordinary differential equations is specific in the framework of hard-constrained DeepONets in several aspects. One of them is the same as for soft-constrained DeepONets, see footnote 2, i.e., there are no sensor points in this case, and the initial or boundary values can be directly used as network inputs. For hard constraints specifically, it is essential that most problems considered for ordinary differential equations are purely initial, without boundary conditions. This necessitates the modification of the ansatz 8 for this setting. More specifically, given a family of initial value problems  $u_t^l - \tilde{\Delta}^l(t, \mathbf{u}) = 0$ ,  $l = 1, \dots, L$ ,  $\mathbf{u}|_{t=t_0} = \mathbf{f}$ , where  $\mathbf{f}$  is a tuple of constant parameters, a possible replacement for (8) is

$$\mathcal{G}^\theta(\mathbf{f})(t) = F_i(t)\mathbf{f} + F_{nn}(t)\mathcal{G}_t^\theta(\mathbf{f})(t), \quad (13)$$

where  $t \in [t_0, t_f]$ ,  $\mathcal{G}_t^\theta$  is the trainable part of the network  $\mathcal{G}^\theta$ , and  $F_i$  and  $F_{nn}$  are fixed sufficiently smooth functions with domain  $[t_0, t_f]$  that satisfy the conditions

$$F_i(t_0) = 1, \quad F_{nn}(t_0) = 0, \quad \frac{\partial F_{nn}}{\partial t}(t_0) \neq 0, \quad F_{nn}(t) \neq 0, \quad t \in (t_0, t_f].$$

Purely boundary problems for systems of ordinary differential equations also require specific hard constraints, see Section 3.2.

### 3 Results

In this section, we demonstrate that DeepONets with hard constraints perform better compared to DeepONets with soft constraints. We first consider two examples with (systems of) ordinary differential equations (ODEs) and then two examples with partial differential equations (PDEs).

In Table 1 we give the details about the setups of each neural network. For the ODE we will employ the hard constraint in the network architecture and for the PDEs we will employ the hard constraint in the loss function. In all problems, we use the Adam optimizer with parameters  $\beta_1 = 0.95$  and  $\beta_2 = 0.99$  with an exponentially decaying learning rate starting at  $10^{-2}$  using 200 decay steps with a decay rate of 0.95. The codes for each example are published on GitHub<sup>4</sup>.

To quantify the error we will use the root mean square error (RMSE) given by

$$\text{RMSE } (u, v) = \sqrt{\frac{1}{N} \sum_{i=1}^N (u - v)^2}. \quad (14)$$

Then, we calculate the improvement percentage of  $u$  over  $v$  by  $100 \frac{|u-v|}{v}$ .

**Remark 3.** One might think that the choice of functions in the hard constraint leads to a better result rather than getting the initial conditions right and being continuous. Moreover, the loss weights for the initial, boundary and residual values could be tuned to optimize the training for the soft-constrained DeepONet. In [17], they tuned the weights for the loss and also modified the architecture of the DeepONet and found that for the advection equation the tuning of weights does not reduce the error significantly, however changing the architecture. We also tested different more complicated functions for the hard constraint which however improve the results. Thus, to have a fair comparison we used the simplest weights for the loss and the simplest function for the hard constraint.

**Remark 4.** One can implement the hard constraint not explicitly in the NN architecture but implicitly in the loss function.

---

<sup>4</sup><https://github.com/RudigerBrecht/hardConstraintDeepONet>

Neural network setup	Lorenz–1963	Poisson	Wave	KdV
Sensor points	3	2	100	100
Coordinates	$t$	$x$	$t, x$	$t, x$
Pre-processing	norm	norm	norm, pb	norm
MLP (units   layers)	60   6	60   6	60   6	60   6

Table 1. Neural network setups for the experiments carried out in this section. Here *norm* refers to normalization of the inputs to the range  $[-1, 1]$  and *pb* indicates the inclusion of periodic boundaries in the neural network architecture.

### 3.1 The Lorenz–1963 model

We consider the family of initial value problems of the Lorenz–1963 model [9] given by

$$\frac{dx}{dt} = \sigma(y - x), \quad \frac{dy}{dt} = x(\rho - z) - y, \quad \frac{dz}{dt} = xy - \beta z, \quad t \in [t_0, t_f], \quad (15)$$

$$x(0) = x_0, \quad y(0) = y_0, \quad z(0) = z_0, \quad (16)$$

where we choose the standard non-dimensional parameters  $\sigma = 10$ ,  $\beta = \frac{8}{3}$  and  $\rho = 28$ . This formulation yields chaotic dynamics. The initial conditions are only parameterized by three constants  $x_0$ ,  $y_0$  and  $z_0$ , and hence  $\Phi = \mathbf{f} = (x_0, y_0, z_0)$ . In other words, there are no sensor points here, and we directly sample values of  $(x_0, y_0, z_0)$  in a compact subset of  $\mathbb{R}^3$ , see Remark 2.

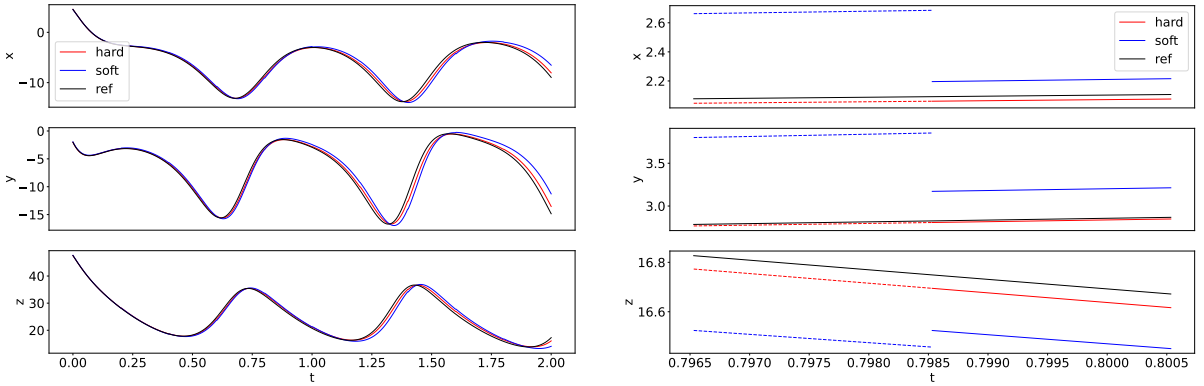
The hard constraint is introduced in the network architecture by

$$\begin{pmatrix} x(t) \\ y(t) \\ z(t) \end{pmatrix} \approx \mathcal{G}^\theta(x_0, y_0, z_0)(t) = \left(1 - \frac{t - t_0}{t_f}\right) \begin{pmatrix} x_0 \\ y_0 \\ z_0 \end{pmatrix} + \frac{t - t_0}{t_f} \mathcal{G}_t^\theta(x_0, y_0, z_0)(t).$$

We train DeepONets with the soft constraint as well as with hard constraints for the interval  $[t_0, t_f]$  with  $t_0 = 0$  and  $t_f = 0.2$ . For the training, we sample 50 000 values for  $(t, x, y, z)$ , where each of  $t$ ,  $x$ ,  $y$  and  $z$  is sampled uniformly in the intervals  $[0, 0.2]$ ,  $[-20, 20]$ ,  $[-25, 25]$  and  $[0, 50]$ , respectively.

We take advantage of the fact that the model under consideration is translation-invariant with respect to  $t$  to use the trained model to perform time-stepping with the step  $\Delta t = 0.2$ , the accuracy of which we use to compare the obtained hard-constrained DeepONet with the standard soft-constrained DeepONet for the problem (15). We would like to emphasize that due to the above invariance, we do not need to modify the network  $\mathcal{G}^\theta$  by means of introducing  $t_0$  as an additional network parameter.

We compare the errors of the two DeepONets for 100 randomly chosen initial conditions after one time step, on the interval  $[0, 0.2]$ , and after 10 time steps, on the interval  $[0, 2]$ . When we evaluate the time stepping with each method and compare it to the corresponding reference solution, we observe that some trajectories significantly differ at some points from the reference solution. This is due the chaotic nature of the Lorenz system. We found that the soft constraint starts to differ for 8% of the trajectories while the hard constraint only differs for 1% of the trajectories. Moreover, when a trajectory computed with the hard-constrained DeepONet deviates from the corresponding reference trajectory, then the trajectory computed with the soft-constrained DeepONet does the same. This is why for computing the error, we only choose trajectories that stay close to the reference solution, see Table 2. In Fig. 2a, we show a numerical simulation for one such trajectory. In Fig. 2b, we demonstrate that the soft constraint



(a) Simulation of a trajectory of the Lorenz 63 system for  $t = 2$ .

(b) Zoomed in region of the computed trajectory where one time step ends and the next begins.

Figure 2. Trajectory of the Lorenz 63 system for the hard and soft constraint and zoomed in region.

Lorenz-1963	RMSE (1 step)	RMSE (10 steps)
Soft constraint	0.0102	0.06828
Hard constraint	<b>0.00131</b>	<b>0.03802</b>
Error reduction	87 %	44 %

Table 2. Normalized root mean square error (RMSE) for the soft and hard constraint simulation of the Lorenz system, and reduction in error obtained by using the hard constraint over the soft constraint, after 1 and 10 time steps corresponding to the time intervals  $[0, 0.2]$  and  $[0, 2]$ .

does not lead to a continuous simulation while the hard constraint ensures that the simulation is indeed continuous. The discontinuities in the simulation of the soft constraint can also be seen in Fig. 2a and they lead to a greater deviation from the reference solution.

### 3.2 Poisson equation

The family of boundary value problem for a one-dimensional Poisson equation on the interval  $[-1, 1]$  with the family of prescribed reference solutions

$$u_{\text{ref}}(x; a, b) = \sin(3x) + ax + b$$

is given by

$$\frac{\partial^2 u}{\partial x^2} = -9 \sin(3x), \quad x \in [-1, 1], \quad u(-1) = u_{\text{ref}}(-1; a, b), \quad u(1) = u_{\text{ref}}(1; a, b).$$

The boundary conditions are parameterized by the pair of constant boundary values,

$$\Phi = \mathbf{g} = (g_-, g_+) = (u_{\text{ref}}(-1; a, b), u_{\text{ref}}(1; a, b)).$$

For training, we sample 10 000 values for  $(a, b)$ , where each of  $a$  and  $b$  is sampled uniformly in  $[-1, 1]$ , and the same number of collocation points in  $[-1, 1]$ . We incorporate the hard constraint by

$$u(x) \approx \mathcal{G}^\theta(\mathbf{g})(x) = g_- \frac{1-x}{2} + g_+ \frac{x+1}{2} + (x+1)(x-1) \mathcal{G}_t^\theta(\mathbf{g})(x).$$

Then, we evaluate the trained network with the hard and soft constraint on 100 randomly chosen values of the pair  $(a, b)$ . The RMSE of the soft-constrained DeepONet is about  $4.4 \cdot 10^{-4}$  while

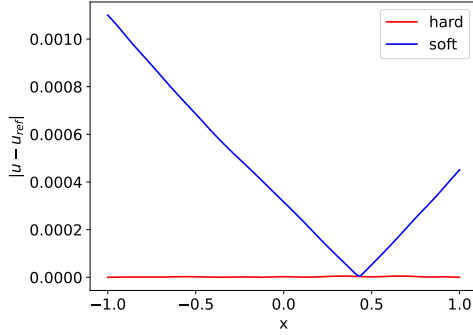


Figure 3. Absolute error of the hard- and soft-constrained solution for the Poisson equation with  $a = 0.3$  and  $b = -0.1$ .

$1.4 \cdot 10^{-5}$  for the hard constraint DeepONet. Thus, the hard constraint improves on the soft constraint by 96%. In Fig. 3, we observe that the hugest difference between the reference and the soft-constrained DeepONet is at the boundary. In contrast to the hard constraint DeepONet, which exactly meets the boundary values.

### 3.3 Linear wave equation

To demonstrate that the hard-approach approach efficiently works for non-evolution equations as well, we apply it to the family of initial boundary value problems for the one-dimensional linear wave equations given by

$$\begin{aligned} \frac{\partial^2 u}{\partial t^2} - \frac{\partial^2 u}{\partial x^2} &= 0, \quad (t, x) \in (0, T) \times (0, 1), \\ u(t, 0) = u(t, 1) &= 0, \quad t \in [0, T], \\ u(0, x) = u_0(x, \mathbf{a}), \quad \frac{\partial u}{\partial t}(0, x) &= 0, \quad x \in [0, 1]. \end{aligned}$$

For the training, we use the parameterized set of initial values in the form of truncated Fourier series,

$$u_0(x, \mathbf{a}) = \sum_{n=1}^3 a_n \sin(n\pi x), \quad \text{where } \mathbf{a} = (a_1, a_2, a_3) \in [-1, 1]^3.$$

The DeepONets are trained until  $T = 1$ .

For evaluation, we use the explicit solution of the problem with  $u(0, x) = \sin(\pi x)$  given by

$$u_{\text{ref}}(t, x) = \cos(\pi t) \sin(\pi x). \quad (17)$$

The initial conditions are parameterized by their values at  $N_s = 100$  evenly spaced sensor points  $x_s^j$ ,  $j = 1, \dots, 100$ , in  $[0, 1]$ , and hence  $\Phi = (u_0(x_s^1, \mathbf{a}), \dots, u_0(x_s^{100}, \mathbf{a}))$ . We implement the hard constraint in the form

$$u(t, x) \approx \mathcal{G}^\theta(\mathbf{a}; \Phi)(t, x) = u_0(x, \mathbf{a}) + t^2 x(x-1) \mathcal{G}_t^\theta(\mathbf{a}; \Phi)(t, x).$$

To sample initial data for training, we sample 10 000 values for  $(a_1, a_2, a_3)$ , where each of  $a_n$ ,  $n = 1, 2, 3$  is sampled uniformly in  $[-1, 1]$ .

In Fig. 4, it is evident that the wave is more accurately represented using the hard-constrained DeepONet in comparison to the soft-constrained DeepONet, particularly noticeable during

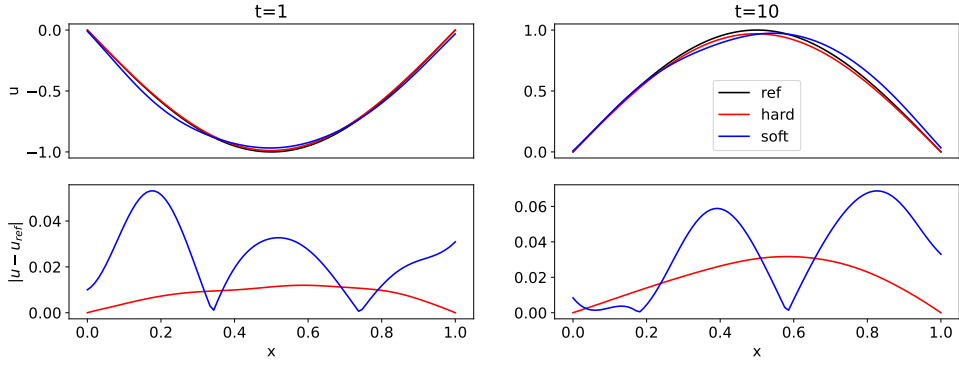


Figure 4. Prediction and error for the simulation of the wave equation. (Top row) Prediction of the wave at time  $t = 1, t = 10, t = 100$  using the model with the soft and hard constraint. (Bottom row) difference of the predicted wave to the reference solution.

lengthier integration intervals. The soft-constrained DeepONet, which only approximates the boundary conditions, has deviations as seen in the error plots, with errors at  $x = 0$  and  $x = 1$ . Conversely, the hard-constrained DeepONet precisely satisfies the boundary conditions, resulting in zero error at these points. The comprehensive errors are assessed using the RMSE, as outlined in Table 3. Across a single integration, the error exhibited by the hard-constrained DeepONet is threefold superior to that of the soft-constrained DeepONet, escalating to fourfold for extended temporal integrations.

Wave	RMSE (1 step)	RMSE (10 steps)
Soft constraint	0.0207	0.026
Hard constraint	<b>0.0057</b>	<b>0.0124</b>
Error reduction	72%	52%

Table 3. Root mean square error (RMSE) for the soft constraint and the hard constraint simulations of the linear wave equation compared with the reference solution, and reduction in error obtained by using the hard constraint over the soft constraint, measured for intervals  $[0, 1]$  and  $[0, 10]$ .

### 3.4 Korteweg–de Vries equation

As the last example, we consider a nonlinear partial differential equation. Specifically, we study a set of initial value problems for the Korteweg–de Vries equations given by

$$\begin{aligned} \frac{\partial u}{\partial t} + \epsilon u \frac{\partial u}{\partial x} + \mu \frac{\partial^3 u}{\partial x^3} &= 0, \quad (t, x) \in [0, T] \times [0, 5], \\ u(0, x) &= u_0(x, a, c) := u_{\text{ref}}(0, x, a, c), \quad x \in [0, 5], \end{aligned}$$

with  $\epsilon = 0.12$  and  $\mu = 0.0008$ . An explicit solution for this equation is given by:

$$u_{\text{ref}}(t, x, a, c) = \frac{c}{2} \text{sech}^2 \left( \frac{\sqrt{c}}{2} \left( 5(x - a) - \frac{ct}{10} \right) \right). \quad (18)$$

For training we set  $T = 10$  and sample different initial conditions  $u_0$  by randomly choosing  $a \in [1, 4]$  and  $c \in [0, 2]$ .

The initial conditions are parameterized by their values at  $N_s = 100$  evenly spaced sensor points  $x_s^j$ ,  $j = 1, \dots, 100$ , in  $[0, 5]$ , and hence  $\Phi = (u_0(x_s^1, a, c), \dots, u_0(x_s^{100}, a, c))$ . The hard

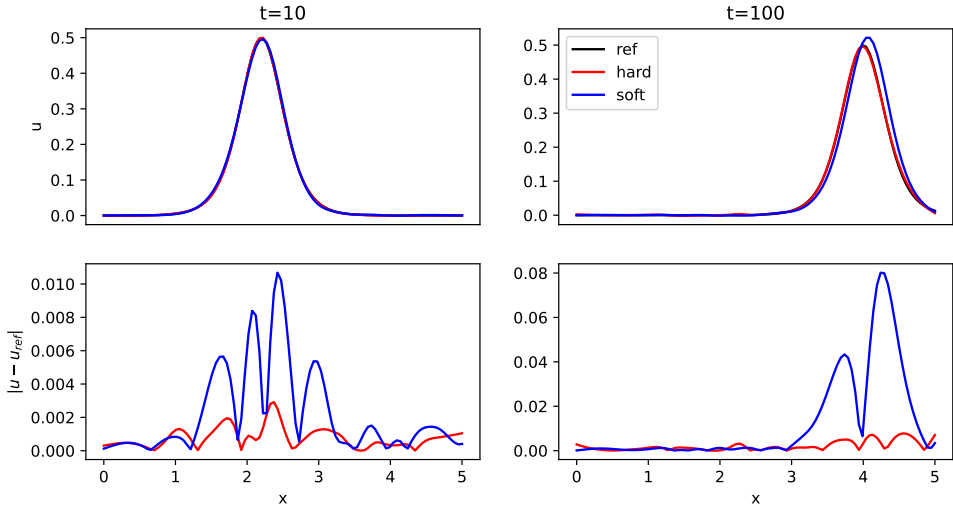


Figure 5. (Top row) Prediction of the wave at time  $t = 10, t = 100$  using the model with the soft and hard constraint. (Bottom row) difference of the predicted wave to the reference solution.

constraint layer is implemented as follows

$$u(t, x) \approx \mathcal{G}^\theta(\Phi)(t, x) = u_0(x, a, c) + \frac{t}{T} \mathcal{G}_t^\theta(\Phi)(t, x).$$

To sample initial data for training, we sample 10 000 values for  $a, c$ , sampled uniformly in  $[1, 4]$  and  $[0, 2]$ .

In Fig. 5 we see the soliton after one and ten time steps. After the first step, the solutions look similar, however the soft-constrained DeepONet produces higher errors compared to the hard-constrained DeepONet. Then, after ten time steps the errors grow strongly for the soft-constrained DeepONet and are about 5 times greater than for the hard-constrained DeepONet, see Table 4.

KdV	RMSE (1 step)	RMSE (10 steps)
Soft constraint	0.00193	0.00927
Hard constraint	<b>0.00091</b>	<b>0.00179</b>
Error reduction	53 %	80 %

Table 4. RMSE for the soft and hard constraint simulation of the KdV equation compared with the reference solution, and reduction in error obtained by using the hard constraint over the soft constraint measured for intervals  $[0, 10]$  and  $[0, 100]$ .

## 4 Conclusions

This study pioneered the integration of a hard constraint initial and/or boundary condition into the architecture or loss function of a physics-informed DeepONet, thereby achieving exact representation of initial and boundary values. This hard constraint inclusion has several advantage. Firstly, it substantially simplifies the optimization problem that has to be solved to train physics-informed DeepONets. This is due to the loss function then reducing to the differential equation loss only, as all initial and/or boundary conditions are automatically satisfied by the model architecture. Secondly, when utilizing the DeepONet to perform time-stepping for a solution, a continuous solution is guaranteed. This is in contrast to the traditional soft-constraint

approach, where the solution will incur jumps when iterative time stepping is carried out. We have illustrated for several examples that the proposed hard-constrained method outperforms the traditional soft-constraint approach.

For the purpose of this paper, we have focused on the simplest form of the hard-constrained DeepONets. Further room for experimentation exists in using more sophisticated ansatzes that incorporate the initial and/or boundary data of a differential equation into the neural network exactly. This may be essential for ensuring not only continuity, but also differentiability of a time-stepped numerical solution using DeepONets.

To the best of our knowledge, DeepONets have rarely been applied to boundary value problems. The standard soft-constrained DeepONet needs to learn the boundary values in order to accurately learn the solution. In contrast, the hard-constraint does not suffer from this problem and achieves much better results.

We should also like to point out that while the hard-constrained DeepONets have generally given lower errors than their soft-constrained counterparts, there may be situations where the soft-constraint approach is more straightforward to implement. This concerns the formulation of problems on irregular domains, which may pose challenges for the hard-constrained version of DeepONets.

## Acknowledgements

This research was undertaken thanks to funding from the Canada Research Chairs program, the NSERC Discovery Grant program and the AARMS CRG *Mathematical foundations and applications of Scientific Machine Learning*. The research of RB is funded by the Deutsche Forschungsgemeinschaft (DFG, German Research Foundation) – Project-ID 274762653 – TRR 181.

## References

- [1] Baydin A.G., Pearlmutter B.A., Radul A.A. and Siskind J.M., Automatic differentiation in machine learning: a survey, *J. Mach. Learn. Res.* **18** (2018), Paper No. 153.
- [2] Bihlo A., Improving physics-informed neural networks with meta-learned optimization, *arXiv preprint arXiv:2303.07127* (2023).
- [3] Bihlo A. and Popovych R.O., Physics-informed neural networks for the shallow-water equations on the sphere, *J. of Comput. Phys.* **456** (2022), 111024.
- [4] Brecht R. and Bihlo A., M-ENIAC: A machine learning recreation of the first successful numerical weather forecasts, *arXiv preprint arXiv:2304.09070* (2023).
- [5] Chen T. and Chen H., Universal approximation to nonlinear operators by neural networks with arbitrary activation functions and its application to dynamical systems, *IEEE Trans. Neural Netw.* **6** (1995), 911–917.
- [6] Krishnapriyan A., Gholami A., Zhe S., Kirby R. and Mahoney M.W., Characterizing possible failure modes in physics-informed neural networks, *Adv. Neural Inf. Process.* **34** (2021), 26548–26560.
- [7] Lagaris I.E., Likas A. and Fotiadis D.I., Artificial neural networks for solving ordinary and partial differential equations, *IEEE Trans. Neural Netw.* **9** (1998), 987–1000.
- [8] Liu M., Liang L. and Sun W., A generic physics-informed neural network-based constitutive model for soft biological tissues, *Comput. Methods Appl. Mech. Eng.* **372** (2020), 113402.
- [9] Lorenz E.N., Deterministic nonperiodic flow, *J. Atmos. Sci.* **20** (1963), 130–141.
- [10] Lu L., Jin P., Pang G., Zhang Z. and Karniadakis G.E., Learning nonlinear operators via DeepONet based on the universal approximation theorem of operators, *Nat. Mach. Intell.* **3** (2021), 218–229.

- [11] Martin J. and Schaub H., Physics-informed neural networks for gravity field modeling of the Earth and Moon, *Celest. Mech. Dyn. Astron.* **134** (2022), 13.
- [12] Raissi M., Deep hidden physics models: Deep learning of nonlinear partial differential equations, *J. Mach. Learn. Res.* **19** (2018), 932–955.
- [13] Song C., Alkhalifah T. and Waheed U.B., Solving the frequency-domain acoustic vti wave equation using physics-informed neural networks, *Geophys. J. Int.* **225** (2021), 846–859.
- [14] Wang S. and Perdikaris P., Long-time integration of parametric evolution equations with physics-informed deepnets, *J. Comput. Phys.* **475** (2023), 111855.
- [15] Wang S., Sankaran S. and Perdikaris P., Respecting causality is all you need for training physics-informed neural networks, *arXiv preprint arXiv:2203.07404* (2022).
- [16] Wang S., Teng Y. and Perdikaris P., Understanding and mitigating gradient flow pathologies in physics-informed neural networks, *SIAM J. Sci. Comput.* **43** (2021), A3055–A3081.
- [17] Wang S., Wang H. and Perdikaris P., Improved architectures and training algorithms for deep operator networks, *Journal of Scientific Computing* **92** (2022), 35.
- [18] Wang S., Yu X. and Perdikaris P., When and why pinns fail to train: A neural tangent kernel perspective, *J. Comput. Phys.* **449** (2022), 110768.